Molecular Mechanism of Water Bridge Buildup: Field-Induced Formation of Nanoscale Menisci

Tobias Cramer,*,† Francesco Zerbetto,*,† and Ricardo García*,‡

Dipartimento di Chimica "G. Ciamician", Università di Bologna, V. F. Selmi 2, 40126 Bologna, Italy, and Instituto de Microelectrónica de Madrid, CSIC, Isaac Newton 8, 28760 Tres Cantos, Madrid, Spain

Received January 23, 2008. Revised Manuscript Received March 18, 2008

We perform molecular dynamics calculations to describe, at the molecular level, the formation of a water bridge induced by an electric field. Restriction of orientational degrees of freedom (confinement) of water dipoles at the interfaces leads to a polarizability that depends on the shape of the water system, that is, droplet versus pillar. Above a threshold field of 1.2 V nm^{-1}, the competition between orientational confinement and electric field leads to the sudden formation of a water pillar. The formation of a water bridge is marked by a first order discontinuity in the total energy of the system. The simulations offer a molecular explanation for the threshold voltage and hysteresis behavior observed in the formation of nanoscale liquid bridges with a force microscope.

Introduction

At ambient pressure and below water saturation, the vicinity of two surfaces can trigger spontaneous capillary condensation followed by formation of a water bridge.[1] The phenomenon occurs even at the nanoscopic level between a surface and an atomic force microscope (AFM) tip,[2] where it may change the dynamic response of the cantilever[3] or lead to energy dissipation.[4] The bridge, in equilibrium with the vapor, forms a concave meniscus of negative mean curvature defined by the Kelvin equation, which seems to be valid for systems down to menisci of radius of 2−4 nm.[5] This is remarkable because lattice gas Monte Carlo simulations showed that thermal fluctuations set the minimum width of a stable meniscus to 5 molecular diameters (1.9 nm) even when the top surface reduces to an atomically sharp tip.[6] The similarity of the dimensions implies the validity of the thermodynamical equation down to the molecular level.

Thermodynamics therefore provides a sound understanding of the morphology of the bridge. However, its manipulation, at the nanoscale, can be both challenging and rewarding because of its practical consequences in the fabrication of structures and devices such as atomic force microscopy based nanolithographies.[7] For instance, in dip-pen nanolithography, the meniscus serves as a channel for molecules to flow from the tip to the substrate, while in local oxidation nanolithography it confines spatially the anodic oxidation. Electric fields offer one of the best experimental approaches to control and manipulate the properties of liquid bridges at the macro-[8] and nanoscale.[9]Using an AFM setup, Gómez-Monivas et al. demonstrated that above a critical field strength E_{th} of 0.7−1.9 V nm^{-1} water bridge formation is induced electrostatically.[10] Considering that the distance between the tip and substrate is several nanometers, the bridge formation seems to be initiated by the deformation of the adsorbed water film under the influence of field-induced polarization.

A significant number of simulations at the continuum level[11] and at the molecular scale[12−14] of interfacial water, with and without external electric fields, exists. Molecular dynamics (MD) simulations of electrowetting of nanosized aqueous droplets on graphite found a high sensitivity of water contact angles to the electric field.[12] The interplay between an electric field and the interfacial hydrogen bond network can even turn a hydrophobic system into hydrophilic.[13] A phenomenon hardly taken into account in continuum approaches.

Here, we provide a description of the interaction of water molecules with an electric field that eventually results in the growth of a water bridge/pillar. The calculations show that the formation of the pillar requires a threshold field of 1.2 V nm^{-1}. In a simple continuum picture, the growth starts when the electrostatic pressure overcomes the surface tension. The pressure

* To whom correspondence should be addressed. Fax: (+39) 051 209 9456. E-mail: francesco.zerbetto@unibo.it (F.Z.); rgarcia@imm.cnm.csic.es (R.G.); tobias.cramer@unibo.it (T.C.).

† Università di Bologna.

‡ Instituto do Microelectrónica de Madrid.

(1) Israelachvili, J. N. *Intermolecular and Surface Forces: With Applications to Colloidal and Biological Systems*, 3rd ed.; Academic: New York, 1998.

(2) (a) Colchero, J.; Storch, A.; Luna, M.; Gomez-Herrero, J.; Baro, A. M. *Langmuir* **1998**, *14*, 2230–2234. (b) Choe, H.; Hong, M. H.; Seo, Y.; Lee, K.; Kim, G.; Cho, Y.; Ihm, J.; Jhe, W. *Phys. Rev. Lett.* **2005**, *95*, 187801.

(3) Stifter, T.; Marti, O.; Bhushan, B. *Phys. Rev. B* **2000**, *62*, 13667–13673.

(4) Sahagun, E.; Garcia-Mochales, P.; Sacha, G. M.; Saenz, J. J. *Phys. Rev. Lett.* **2007**, *98*, 176106.

(5) (a) Fisher, L. R.; Israelachvili, J. N. *Colloids Surf.* **1981**, *3*, 303–319. (b) Christenson, H. K. *Phys. Rev. Lett.* **1994**, *73*, 1821–1824. (c) Digilov, R. *Langmuir* **2000**, *16*, 1424–1427. (d) Sirghi, L.; Szoszkiewicz, R.; Riedo, E. *Langmuir* **2006**, *22*, 1093–1098.

(6) Jang, J.; Schatz, G. C.; Ratner, M. A. *Phys. Rev. Lett.* **2004**, *92*, 085504.

(7) (a) Garcia, R.; Calleja, M.; Rohrer, H. *J. Appl. Phys.* **1999**, *86*, 1898–1903. (b) Lyuksyutov, S. F.; Vaia, R.; Paramonov, P. B.; Juhl, S.; Waterhouse, L.; Ralich, R.; Sigalov, G.; Sancaktar, E. *Nat. Mater.* **2003**, *2*, 468–471. (c) Cai, Y. G.; Ocko, B. M. *J. Am. Chem. Soc.* **2005**, *127*, 16287–16291. (d) Xie, X. N.; Chung, H. J.; Liu, Z. J.; Yang, S.-W.; Sow, C. H.; Wee, A. T. S. *Adv. Mater.* **2007**, *19*, 2618–2623. (e) Schmitz, M. J.; Kinser, C. R.; Cortes, N. E.; Hersam, M. C. *Small* **2007**, *3*, 2053–2056. (f) Lee, W.-K.; Caster, K. C.; Kim, J.; Zauscher, S. *Small* **2006**, *2*, 848–853. (g) Liu, X.; Shouwu, G.; Mirkin, C. A. *Angew. Chem.* **2003**, *115*, 4933–4937. (h) Liu, X.; Shouwu, G.; Mirkin, C. A. *Angew. Chem., Int. Ed.* **2003**, *42*, 4785–4789.

(8) Fuchs, E. C.; Woisetschläger, J.; Gatterer, K.; Maier, E.; Pecnik, R.; Holler, G.; Eisenköbl, H. *J. Phys. D* **2007**, *40*, 6112–6114.

(9) (a) Calleja, M.; Tello, M.; Garcia, R. *J. Appl. Phys.* **2002**, *92*, 5539–5542. (b) Garcia-Martin, A.; Garcia, R. *Appl. Phys. Lett.* **2006**, *88*, 123115. (c) Sacha, G. M.; Verdaguer, A.; Salmeron, M. *J. Phys. Chem. B* **2006**, *110*, 14870–14873.

(10) Gómez-Monivas, S.; Sáenz, J. J.; Calleja, M.; García, R. *Phys. Rev. Lett.* **2003**, *91*, 056101.

(11) (a) Girault, H. H. *Nat. Mater.* **2006**, *5*, 851–852. (b) Monroe, C. W.; Daikhin, L. I.; Urbakh, M.; Kornyshev, A. A. *Phys. Rev. Lett.* **2006**, *97*, 136102.

(12) Daub, C. D.; Bratko, D.; Leung, K.; Luzar, A. *J. Phys. Chem. C* **2007**, *111*, 505–509.

(13) Bratko, D.; Daub, C. D.; Leung, K.; Luzar, A. *J. Am. Chem. Soc.* **2007**, *129*, 2504–2510.

(14) (a) Joshi, R. P.; Qian, J.; Schoenbach, K. H.; Schamiloglu, E. *J. Appl. Phys.* **2004**, *96*, 3671–3624. (b) Yang, K.-L.; Yiacoumi, S.; Tsouris, C. *J. Chem. Phys.* **2002**, *117*, 337–345. (c) Shevkunov, S. V.; Vegiri, A. *J. Mol. Struct.* **2002**, *593*, 19–32. (d) Yeh, I.-C.; Berkowitz, M. L. *J. Chem. Phys.* **2000**, *112*, 10491–10495.

10.1021/la800220r CCC: $40.75
Published on Web 05/17/2008

is caused by a variation of permittivity that originates from the restriction of the rotational degrees of freedom of interfacial water molecules that, however, conserve the hydrogen bond network. Our findings are consistent with the experimental measurements and complement the phenomenological description provided by macroscopic models.

Methods

We perform molecular dynamics simulations in the NVT-ensemble using the SPC/E potential for water[15] and a modified version of the Tinker-Program Package.[16] We assume that water is adsorbed on a polar surface, which is simulated by a 3-9 potential. The coefficient of the attractive term is derived from the Hamaker constant of water on silicon dioxide, 1.1×10^{-19} J, and is 22.6 kcal Å^3 mol^{-1}. The repulsive term, 400.0 kcal Å^9 mol^{-1}, is chosen to reproduce the contact angle of water on the same surface, namely, ~40°. The molecular dynamics were run at constant temperature from a sample of 1014 water molecules equilibrated for 500 ps on the planar surface. To minimize water evaporation, a simple reflecting boundary was enforced. The shake-up algorithm was used to freeze the internal degrees of freedom of the molecules. The external electric field interacts with the point charges of the SPC/E−water model. In order to compare the field strength to the experimentally applied potential between an AFM tip and the surface, we used a model based on a planar capacitor geometry. The surface of the droplet is calculated by the "rolling ball" algorithm. As the probe radius, we used a value of 1.4 Å. Molecules that contribute to this surface are considered as interfacial molecules in further calculations. In order to assign hydrogen bonds, we used a definition that is based on the relative geometry between two water molecules and gives reliable results in simulations.[17] This definition requires the oxygen−oxygen distance to be less than 3.5 Å and the O−H···O angle to be less than 30°.

Results and Discussion

In our molecular dynamics simulation, the water droplet was subjected to electric fields in the range between +0.25 and +2.25 V nm^{-1}, with steps of 0.25 V nm^{-1}. As an example, Figure 1 shows three snapshots from the formation of a pillar of molecules induced by a field of 2.00 V nm^{-1}. The simulation starts from a configuration (droplet) equilibrated in the absence of the field, where the average contact angle on a silicon dioxide surface is 40° (Figure 1a). The field perpendicular to the surface polarizes and distorts the outermost water layer. The drop changes shape (Figure 1b), and finally a water pillar is formed (Figure 1c). As a parameter to monitor the change of the drop shape, we use the size perpendicular to the surface (height), $h_z = [(1/N)\Sigma_i(z_i - \langle z\rangle)^2]^{1/2}$, where N is the number of molecules and z_i is the molecule's distance from the surface. The change of h_z as a function of time for different field strength is shown in Figure 1d. At 2.25, 2.00, 1.75, 1.50, and 1.25 V nm^{-1}, the shape of the droplet starts to change immediately. In contrast, no tendency to form a column was observed at 1.0 V nm^{-1} even at longer time scales (up to 1.0 ns, data not shown). The kinetics of the displacement, h_z, is sigmoidal in time. This behavior follows from the presence of limiting factors during the growth process, such as the tensile strength of water.[18]

In order to rationalize the threshold behavior, we analyzed the total energy, U_{total}, of the equilibrated system as a function of the electric field. Figure 2a shows that in the droplet U_{total} varies only slightly, while in the pillar the energy decreases with increasing field. This first order discontinuity in total energy renders the droplet metastable once the field is above the threshold and the pillar is formed. Notice that self-diffusion in these confined geometries may differ substantially from the behavior in the

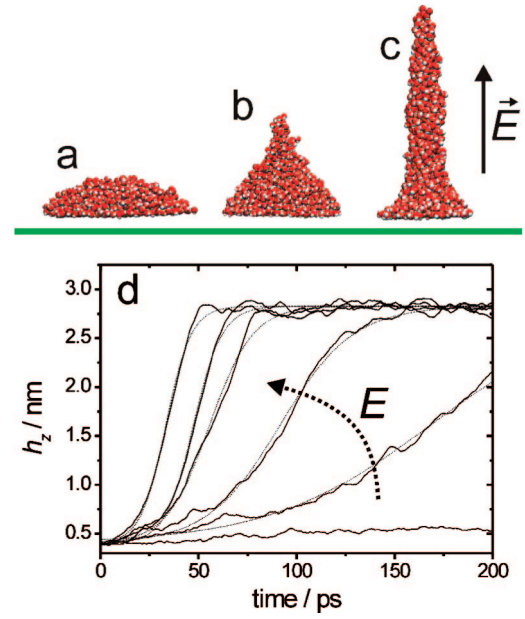

Figure 1. MD evolution of 1014 SPC/E water molecules in the presence of an external electric field on a hydrophilic surface. Snapshots from the simulation at $E_z = 2.0$ V nm^{-1}(oxygen, red; hydrogen, white): (a) equilibrated state without field; (b) 35 ps after switching on the field; and (c) final equilibrated state ($t = 75$ ps). (d) Height increase as a function of time for six values of the electric field (2.25, 2.0, 1.75, 1.5, 1.25, and 1.0 V nm^{-1}) (lines) and fit to sigmoidal function (dotted lines).

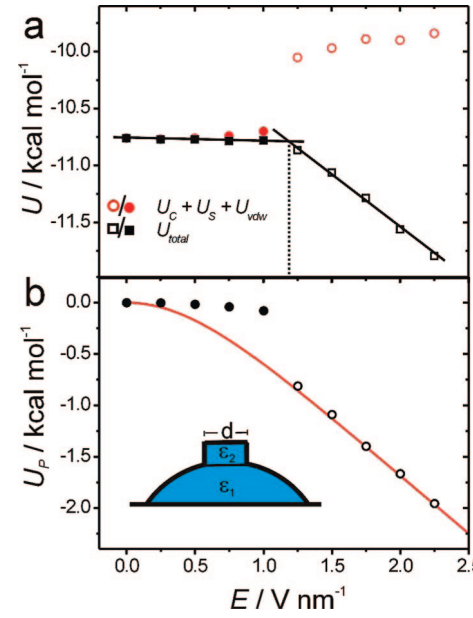

Figure 2. Influence of the field strength on averaged energy components. (a) Total energy U_{total} (squares) and sum of water internal components (circles, U_C, U_S, U_{vdw}; see text for details). The threshold field strength for the transition into the column configuration (open symbols) is indicated by the dotted line ($E_{th} = 1.2$ V nm^{-1}). (b) Polarization energy U_P for the simulated system (circles) and for unrestricted dipoles following the Langevin equation (line). The inset represents the continuum model for the rationalization of the column growth.

(15) Berendsen, H. J. C.; Grigera, J. R.; Straatsma, T. P. *J. Phys. Chem.* **1987**, *91*, 6269–6271.
(16) Ponder, J. W.; Richards, F. M. *J. Comput. Chem.* **1987**, *8*, 1016–1024.
(17) (a) Starr, F.; Nielsen, J.; Stanley, H. *Phys. Rev. B* **2000**, *62*, 579–584. (b) Kumar, R.; Schmidt, J. R.; Skinner, J. L. *J. Chem. Phys.* **2007**, *126*, 204107.
(18) Lugli, F.; Höfinger, S.; Zerbetto, F. *J. Am. Chem. Soc.* **2005**, *127*, 8020–8021.

Table 1. Properties of Liquid Water: Values Used by Gómez-Monivas et al.[10] in Their Continuum Model and Calculated Values for The SPC/E Water Model Used Here

	SPC/E	experimental/continuum model
surface tension γ	64 mJ m^{-2}	73 mJ m^{-2}
density (25 °C) ρ	0.998 g cm^{-3}	0.995 g cm^{-3}
permittivity ε	68.2 ± 5.8	79.0
Hamaker constant A	11 × 10^{-20} J m	11 × 10^{-20} J m
contact angle Θ	40°	0°
evaporation enthalpy $\Delta_v H$	11.4 kcal mol^{-1}	10.52 kcal mol^{-1}

bulk.[19] The mobility of individual water molecules remains roughly constant during the shape transition, which implies a similar entropic contribution in the two conformations. We extrapolate the curves for the two shapes to obtain a threshold field of 1.2 V nm^{-1}, which agrees with the experimental range of values $E_{th} = 0.7-1.9$ V nm^{-1}.[9,10] The inhomogeneous field decay due to the AFM tip curvature causes the experimental uncertainty.

In our simulation, the contributions to the total energy come from four interactions: (i) the electrostatic interaction between water molecules, U_C, (ii) the van der Waals interaction between water molecules, U_{vdw}, (iii) the interaction of water molecules with the hydrophilic surface, U_S, and (iv) the interaction with the external field due to polarization of the water molecules, $U_P = -E_z\mu\langle\cos\Theta\rangle$, where Θ is the angle between the dipole μ and the electric field, E_z. The water internal contributions U_C and U_{vdw} and the interaction with the solid surface U_S increase during the shape transition (Figure 2a). The driving force for the shape transition is the reduced polarization energy U_P in the pillar. Its dependence on the external field can be compared to the Langevin case, where a single dipole interacts with the field and is only disturbed by thermal motion, without any other restrictions due to an intermolecular potential:

$$U_{P,L} = -E_z\mu\left[\coth\left(\frac{\mu E}{k_B T}\right) - \frac{k_B T}{\mu E}\right] \quad (1)$$

Using the dipole moment of the SPC/E water molecule, one obtains a perhaps surprisingly good agreement between eq 1 and U_P in the pillar configuration (Figure 2b, empty circles). Instead, in the droplet, the polarization of the water dipoles is reduced (Figure 2b, filled circles) and eq 1 is not fulfilled. We conclude that the dipole reorientation is strongly restricted in the droplet.

The mechanism of column formation can be rationalized by a simple continuum picture (see inset of Figure 2b). In an electric field, a pressure is created between two dielectric materials of different permittivities. The effect has, for example, been used to explain surface instabilities in liquid polymer films.[20] The difference of the polarization energies ΔU_P of the two configurations corresponds to a change in permittivity. The pressure in the direction of the external field can be calculated by assuming that the system behaves as a linear dielectric material:

$$p_E = \frac{1}{2}\Delta\varepsilon\varepsilon_0 E^2 = \Delta U_P n \quad (2)$$

where n is the number density of liquid water. Extrapolation of Figure 2b gives, at the threshold field, $\Delta U_P = 0.67$ kcal mol^{-1}, which corresponds to $\Delta\varepsilon \approx 27$. For the rise of a column of diameter d, the Laplace pressure due to the surface tension $p_\gamma = -4\gamma/d$ has to be exceeded. At the threshold field, the two pressures balance one another and E_{th} can be estimated: $E_{th} = (8\gamma/\Delta\varepsilon\varepsilon_0 d)^{1/2}$. Using $\gamma = 70$ J m^{-2} (Table 1) and $d = 1.9$ nm (s.o.) gives $E_{th} \approx 1.1$ V nm^{-1}, which is consistent with the MD result.

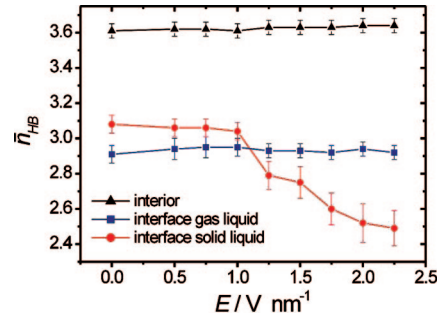

Figure 3. Average number of hydrogen bonds per water molecule as a function of the field strength. Above $E = 1.2$ V nm^{-1}, the sample is in the column conformation.

In the following, we investigate the liquid structure in order to explain the difference in rotational restriction in the two droplet conformations. First, we analyze the average number of hydrogen bonds per water molecule, $\bar{n}_{HB}$, as a function of the field strength. For the averaging, we distinguished between molecules that reside at one of the two different interfaces or in the interior, bulklike parts of the droplet. Figure 3 shows that $\bar{n}_{HB}$ for molecules in the bulk and at the liquid−gas interface display only minor fluctuations when the field is increased and even the shape transition at 1.2 V nm^{-1} has no effect. Only the few molecules that are at the interface with the solid surface show a different behavior. This case is discussed below. The average values are $\bar{n}_{HB} = 3.63 \pm 0.04$ in the interior and $n_{HB} = 2.93 \pm 0.04$ at the liquid−gas interface. A similar response has already been described in studies based on molecular simulations and on statistical models.[21–23] Albeit the absolute values for $\bar{n}_{HB}$ depend on the definition of hydrogen bond, also these works show no significant influence on hydrogen bonding for fields below ~5 V nm^{-1}.[22] Further evidence that the system maintains the hydrogen bond network comes from the oxygen−hydrogen pair correlation function. For the droplet and for the column conformation, it exhibits the characteristic features of the hydrogen bond network of the SPC model (peaks at 0.18 and 0.34 nm; see the Supporting Information).

From these findings, we conclude that the first coordination shell of the water molecules remains nearly undisturbed by the field and the system fulfills the requirement of conserving the hydrogen bond network. Over the applied field range, the local structure can be regarded as more or less tetrahedral with three to four hydrogen bonds per molecule. The electric field changes the average orientation of the dipoles with respect to the laboratory frame and hence leads to polarization; however, in the local frame of a water molecule, the geometry remains intact. The collective ordering in the field is not in contradiction with local tetrahedral coordination. Instead, due to the C_{2v} symmetry of the molecule, it is even predicted that stronger fields lead to an increased hydrogen bonding[21–23] and finally electrofreezing[24] of the liquid. In conclusion, changes in the liquid structure are not at the origin of the observed change in restriction of the rotational degrees of freedom during the pillar formation.

To investigate if the rotational restriction is interface-induced, we calculated the dipole distribution function for interfacial

(19) Liu, P.; Harder, E.; Berne, B. J. *J. Phys. Chem. B* **2004**, *108*, 6595–6602.
(20) Lin, Z.; Kerle, T.; Baker, S. M.; Hoagland, D. A.; Schäffer, E.; Steiner, U.; Russell, T. P. *J. Chem. Phys.* **2001**, *114*, 2377–2381.
(21) Xia, X.; Berkowitz, M. L. *Phys. Rev. Lett.* **1995**, *74*, 3193–3196.
(22) Kiselev, M.; Heinzinger, K. *J. Chem. Phys.* **1996**, *105*, 650–657.
(23) Suresh, S. J.; Satish, A. V.; Choudhary, A. *J. Chem. Phys.* **2006**, *124*, 074506.
(24) (a) Svishchev, I. M.; Kusalik, P. G. *J. Am. Chem. Soc.* **1996**, *118*, 649. (b) Zangi, R.; Mark, A. E. *J. Chem. Phys.* **2004**, *120*, 7123–7130.

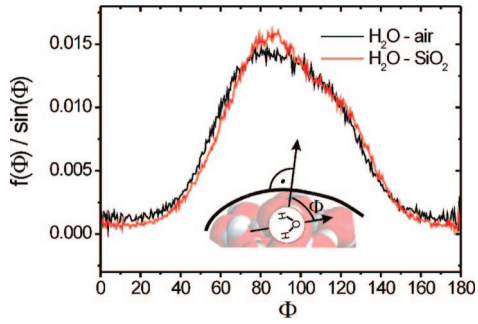

Figure 4. Alignment of the water molecules at the drop interfaces at 0 V nm^{-1} (red, silicon dioxide surface; black, air interface). The angle Φ is between the dipole moment of a water molecule and the normal to the surface; see the inset. The distribution is normalized by sin(Φ) to account for the purely statistical probability.

molecules. Figure 4 shows the distributions at the water−gas and water−solid interfaces at zero field. The distribution has a maximum for the dipoles roughly parallel to the interfaces. In this preferred alignment, three of the four hydrogen bond acceptors/donors are oriented toward the bulk and participate in the hydrogen bond network.[25] This rotational restriction leads to an anisotropic polarizability with respect to the interface normal: If the field is perpendicular to the interface normal, orientational polarization is accompanied by a breaking of the hydrogen bond network.

A combination of the findings of Figures 3 and 4 enables us to give a molecular interpretation of the threshold effect and the accompanying electrostatic pressure. In the droplet configuration, most of the water interface is oriented perpendicular to the field. As a consequence, also the orientation of the dipoles is restricted and they cannot align with the field. The polarizability of a system that cannot react to an electric field is low. At the threshold field, the outermost dipoles start aligning with the field. The alignment could weaken the hydrogen bonds with the molecules underneath. However, the alignment also triggers a domino process that ends with the formation of the water bridge. In this configuration, most of the interface is parallel to the field. In this way, the system fulfills the double requirement of retaining the interfacial hydrogen bond network and allowing orientational polarization.

An insightful exception to the invariability of the hydrogen bonding occurs to the few molecules that are at the solid−liquid interface (see Figure 3). Here, the average number of hydrogen bonds starts to decrease once the field exceeds the threshold. Since this interface is constrained to be perpendicular to the field, the system can no longer fulfill the double requirement of keeping the hydrogen bond network and allowing orientational polarization. Above the threshold, the polarization force starts to prevail over the interfacial hydrogen bonds that wants the dipoles oriented parallel to the interface. Hence, the average number of hydrogen bonds decreases (note that during shape transition also the amount of molecules at the solid−water interface is reduced considerably).

Regarding the stability of the hydrogen bond network, it is interesting to consider why the polarizability of the column conformation is nonetheless well-described by the Langevin equation (eq 1). Free rotation of a single molecule is hindered by the hydrogen bonding with its first coordination shell. However, the system remains in the liquid state, and therefore, the distribution of dipoles is in thermal equilibrium and governed by Boltzmann statistics, which ultimately yields the Langevin

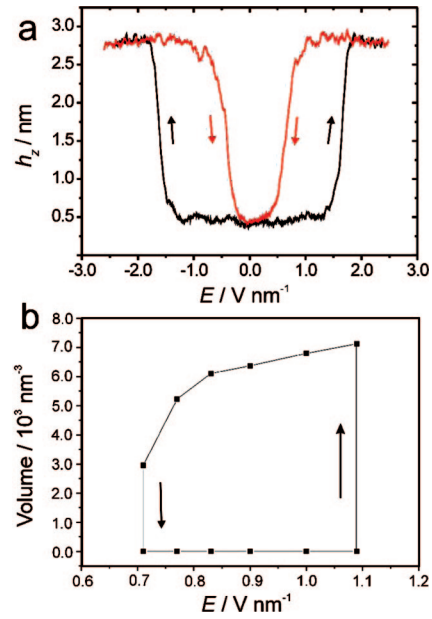

Figure 5. (a) Simulated hysteresis effects during column formation. The electric field is varied with 4.0 V nm^{-1} ns^{-1}; arrows indicate the scan direction. The height of the nanodroplet in the direction perpendicular to the surface. (b) Hysteresis values of the bridge formation at a relative humidity of 30% (adapted from ref 10).

formula. For macroscopic dipolar liquids, this methodology is not applicable, as one neglects, in this way, the long-range correlations due to dipole−dipole interactions. It has been shown[26] that water dipole correlations have a range of around 1.5 nm. The axial radius of the water pillar is below this range ($r \sim 1.0$ nm), and therefore, we suppose that correlation effects are reduced so that the Langevin equation gives an accurate description of the dielectric response.

Besides the threshold field strength, at which the column starts to rise, experiments provide a lower field strength at which the meniscus breaks.[9,10] The effect has a dynamic response as a function of the field (hysteresis). To investigate the dynamic response of the water column to a varying field, we performed a simulation in which the electric field was varied at a rate of 4.0 V nm^{-1} ns^{-1}. Figure 5a shows the structural displacement h_z for scans with increasing and decreasing field strength. Pillar formation sets in at 1.3 V nm^{-1}, close to the extrapolated value for $E_{th} = 1.2$ V nm^{-1}, and the plateau of the pillar height is reached at 1.7 V nm^{-1}. The reverse scan finds that the collapse field is substantially lower at 0.9 V nm^{-1}. The calculated metastability of the column configuration can be related to the hysteresis effects observed in AFM experiments and continuum model simulations (Figure 5b).[9,10]

The present MD simulations are in good qualitative and quantitative agreement with the experiments. They show that a water droplet can be manipulated by an electric field to form a pillar that is similar in appearance to that observed in AFM experiments.[9,10] Two important differences exist between the present simulations and the experiments. The first is the lack of the tip in the calculations. The absence in the simulations of a top surface proves that the field is able to manipulate the liquid and can therefore exert an action when it forms spontaneously a meniscus. The influence on the calculated threshold field strength is negligible, as the exerted dispersion force is orders of magnitude lower than the electrostatic pressure at typical experimental tip

(25) Lee, C.-Y.; McCammon, J. A.; Rossky, P. J. *J. Chem. Phys.* **1984**, *80*, 4448–4455.

(26) Mathias, G.; Tavan, P. *J. Chem. Phys.* **2004**, *120*, 4393–4403.

distances (>5 nm).[27] It has been shown that at closer distances (<4 nm) interactions with local charged surface groups come into play.[28] This is an effect that is neglected in our approach. The second difference is the existence of an initial drop in the calculations, while in the experiments condensation occurs from the air. The presence of the drop can be considered equivalent to assume a relative humidity above 80% and a wetted surface or a surface bound water film. However, due to the hydrophilicity of the surface, a water film can also be expected at lower humidity.[29]

A simple explanation of the consistency of the results of the present calculations and AFM experiments is in the physics underlying the present model. Table 1 lists a set of macroscopic parameters derived for this approach and compares them with the values used by Gómez-Monivas et al.[10] in their continuum model to rationalize the AFM experiments. The similarity of the values implies that the long-time physical behavior of the molecular dynamics and the continuum model should be similar.

The molecular dynamics calculations provide an explanation of the threshold behavior observed in field-induced liquid bridge formation. The rise of a pillar is induced by an electrostatic pressure that overcomes surface tension at the critical field strength. The increased permittivity of the pillar is a consequence of the interface orientation parallel to the field. In this way, the molecular dipoles reorient without decreasing the amount of hydrogen bonds. The predicted threshold field of 1.2 V nm^{-1} agrees with the experimental values. Furthermore, the simulations reproduce the hysteresis behavior also observed experimentally.

Acknowledgment. This work was supported by the European Commission (BIODOT NMP4-CT-2006-032652) and Ministerio de Educación y Ciencia (MAT2006-03833).

Supporting Information Available: Plot showing the oxygen−hydrogen pair distribution function, g_r(OH). This material is available free of charge via the Internet at http://pubs.acs.org.

LA800220R

(27) To estimate an upper value for the dispersion force exerted by the AFM tip, we assume that the tip is planar, infinite and at a distance h to the droplet. The potential due to dispersion is then $U_s = a_H (h - z)^{-3}$, where a_H is a constant whose value can be derived from the experimental Hamaker constant of silicon ($a_H = 22.6$ Å^3 kcal/mol). The force exerted on water can then be obtained by integrating over its volume and subsequently deriving with respect to z. This leads to a pressure of $p_{dis} = 4a_H n/h^3 = 1.7 \times 10^4$ J/m^3 at $h = 5$ nm, which has to be compared to $p_E = \Delta U_P n = 1.5 \times 10^8$ J/m^3 at E_{th}.

(28) Wensink, E. J. W.; Hoffmann, A. C.; Apol, M. E. F.; Berendsen, H. J. C. *Langmuir* **2000**, *16*, 7392–7400.

(29) Szoszkiewicz, R.; Riedo, E. *Phys. Rev. Lett.* **2005**, *95*, 135502.